Kinetic Study of the Devitrification of Mold Powder Slags

Yadira G. Maldonado, F. Andrés Acosta, A. Humberto Castillejos and Brian G. Thomas*
Department of Metallurgical Engineering
Centre for Research and Advanced Studies, CINVESTAV – Unidad Saltillo
Carr. Saltillo-Monterrey Km. 13.5, Ramos Arizpe, 25900
Coahuila, México
Tel.: +52-844-438-9600
Fax: +52-844-438-9610
E-mail: humberto.castillejos@cinvestav.edu.mx
*Department of Mechanical Science and Engineering
University of Illinois at Urbana-Champaign
1206 West Green Street, Urbana, IL 61801
Tel.: 217-333-6919
Fax: 217-244-6534
E-mail: bgthomas@uiuc.edu

Key words: Mold powders, Devitrification, Kissinger type rate equation, TTT diagrams, DTA, Continuous Casting

ABSTRACT

Due to the rapid cooling of the slag infiltrated into the mold-strand gap, it is expected that the rate of devitrification of the glass formed plays a key role in determining the proportion of crystalline phases influencing mold heat transfer. In this investigation, a novel procedure to calculate Time-Temperature-Transformation (TTT) curves of mold slags is presented. It is based on the integration under isothermal conditions of a Kissinger-type rate equation using rate parameters determined from differential thermal analysis (DTA). The estimated TTT curves agree very well with transformations observed metallographically by inspecting glass disks, 3 mm thick, quenched after isothermal treatment. In the latter tests a transverse face of a glass disk, insulated laterally, was seated onto an inductively heated metallic plate subjected to prescribed thermal cycles. Both procedures were found suitable for evaluating and comparing the rate of devitrification exhibited by different mold fluxes.

INTRODUCTION

Within the continuous casting machine the mold is the most crucial component. The rate and uniformity of the heat extracted from the strand in the mold especially near the meniscus is ultimately responsible for the surface quality of the product and the productivity of the machine. An excessive and/or uneven rate of heat extraction from the newly-solidified shell will result in thermally-induced stresses that may ultimately cause longitudinal cracks.[1] On the other hand, insufficient mold heat removal may lead to a relatively weak shell that may bulge or tear upon exiting the mold.[2] The phenomena occurring in the inter-space between the mold and the solidifying shell, i.e., the formation of the air gap and of the solid and liquid slag layers, control heat transfer and lubrication in the process and therefore are the key to the prevention of cracks and other defects.[3]

The crystallization tendency of the solid slag layer has a large influence on mold heat transfer. A large tendency to form crystalline phases has been reported to be beneficial in the casting of peritectic grades since a large crystalline fraction reduces the mold heat flux alleviating longitudinal cracks.[4] The opposite tendency to resist devitrification and remain glassy is required for high speed casting of low carbon steels to decrease the possibility of sticking type breakouts.[4] The influence of crystalline phases on heat transfer is attributed to: formation of pores in the solid layer as a result of the contraction experienced during its formation from the glass phase,[5] widening of the air gap as another result of that contraction[6,7] and scattering of radiation by the crystals which reduces the radiative portion of the heat flux.[8] Thus, the study of the formation of crystalline phases in the slag layer in the mold-strand gap deserves great attention.

Feldbauer et al.[9] pointed out that crystallization of mold slags occur according to a TTT diagram, which is a plot of the isothermal temperature as a function of time needed to crystallize the melt at that temperature. The diagram has a nose shape where the tip corresponds to the temperature, T_n, where the melt, when held isothermally, crystallizes in the shortest possible time (t_n, nose time). A schematic TTT diagram is shown in Figure 1. The slope of the straight line from the liquidus temperature, T_l, to the tip of the nose suggests the critical cooling rate for glass formation, $|\phi_c|$ $(=(T_l - T_n)/t_n)$. This cooling rate is a measure of the ability of a melt to form glass and indicates the slowest rate at which the melt can be cooled from its liquidus temperature without detectable crystallization. The temperature of the hot face of a copper plate slab mold is estimated to range between 200°C and 450°C in CSP thin slab molds[10] and still lower in conventional molds[11] and the steel shell surface is between the liquidus steel temperature and around 1000°C and 1150°C in thin[12] and conventional[2] molds, respectively. It might be expected that the liquid slag infiltrating into the mold-strand inter-

space should solidify as a glassy layer closer to the mold face where the cooling rates are $> |\phi_c|$ and as a crystalline layer towards the strand surface, where possibly the cooling rates are $< |\phi_c|$. However, as O´Malley and Neal[13] and several others have observed the actual layering found in flux films recovered from commercial operations is opposite: the crystalline layer appears on the mold side. The glassy flux film that forms during initial contact with the mold wall remains there long enough to devitrify even though its temperature is low so diffusion is slow. The glass persists near the strand, where temperature is high, perhaps because the undercooling driving force is low. Cooling trajectories for classical crystallization and devitrification are illustrated in Figure 1; the starting points for the trajectories are temperatures equal or above the liquidus temperature of the slag and temperatures below the glass transition temperature, respectively.

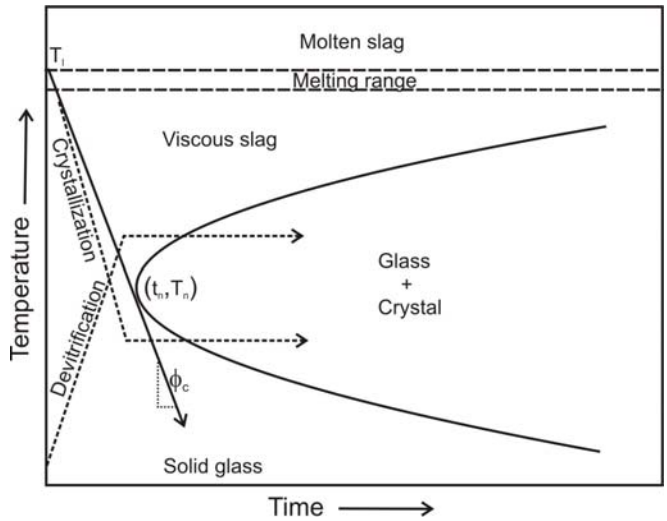

Fig. 1 – Schematic of a typical nose-shaped TTT diagram showing the melting range, the temperature and time corresponding to the nose tip, the critical cooling rate, a cooling trajectory for crystallization and a heating trajectory for devitrification.

Since the TTT diagrams for glass forming materials quantify how the phase transformations evolve with temperature history they are useful tools for designing and selecting mold fluxes. Time-temperature-transformation curves have been studied by several researchers using different thechniques.[14-16] In general, these techniques consist of melting and holding a slag sample at an elevated temperature above its melting point before interrupted quenching to the test temperature where it is held for a specified holding time. The sample is then quenched and inspected for crystalline phases. Repeating this procedure for different isothermal temperatures and holding times generates temperature versus time data to map formation of the first crystals as a TTT curve for the onset of crystallization. Rocabois et al.[14] used a resistance furnace to melt and homogenize oxide mixtures in small sealed crucibles before transferring them to a cooler zone of the furnace for isothermal holding. The cooling rate to reach the isothermal temperature was about 20°C/s. After the holding period the sealed crucibles were water quenched; the operation from the end of isothermal treatment to quenching took approximately 5-10 s. The sample was then cut and the presence of crystals was detected by optical or electronic microscopy. To obtain higher cooling rates, in excess of 150°C/s, and observe the emerging crystals in-situ single and double hot thermocouple techniques have been developed.[15-16] Even higher cooling rates, up to 1000ºC/s, are possible using an impulse atomization process.[17] These techniques enable information on crystallization under both isothermal and non-isothermal conditions.

The construction of TTT curves from isothermal cooling experiments is a very laborious task. A convenient alternative is differential thermal analysis (DTA). However, this method is limited to slow cooling rates, no more than ~1°C/s.[16] A more fundamental problem for using DTA to study the crystallization behavior is that certain melts, particularly those rich in silica, exhibit crystallization peaks that are difficult to discern, due to slow crystallization kinetics or small heats of crystallization.[18] However, the crystallization peaks under devitrification are normally very clearly detectable and have been useful to study the sequential formation of crystalline species from solid glass slags,[18,19] and to estimate the glass fraction present in solid slag films.[20] Property measurements and characterization of mold powder slags as done by Meng et al.[17] become very critical for their design and selection in demanding processes, such as high-speed thin slab casting.[21-23]

From the previous review it is seen that devitrification plays an essential role in the formation of crystalline phases in the solid slag layer located between the strand and the mold. This work presents a novel procedure to calculate TTT curves, which is based on the integration of a Kissinger-type rate equation under isothermal conditions and on the determination of the rate parameters using differential thermal analysis (DTA). The estimated TTT curves agree very well with metallographically determined transformations of glass samples treated isothermally. The kinetic model plus the kinetic information obtained by DTA constitute a powerful combination that simplifies the generation of TTT diagrams.

EXPERIMENTAL TECHNIQUE

Materials

Two commercial mold powders, denoted as A and B, in bags of 25 kg were decarburized in batches of 100 g in porcelain lab dishes. Six dishes at a time were introduced in a muffle at 650°C for 16 hrs, removing the dishes after 5 and 10 hours to mix their charges to ensure complete decarburization. The decarburized powder was ground in an alumina balls mill to a mesh of -100 (-149 μm). The entire amounts of powders A and B were sealed in buckets with desiccant material. The nominal composition of these mold powders is given in Table I.

Table I – Basicity and composition of mold powders A and B.

Powder	$\%CaO/\%SiO_2$	$\%SiO_2$	%CaO	%MgO	$\%Al_2O_3$	$\%(Na_2O+K_2O)$	$\%Fe_2O_3$	%MnO	$\%C_{free}$	%F
A	1.03-1.15	28-30	31-33	2-3.5	5-6.5	8.5-10	< 1.5	2-3.5	2-3.5	7-9
B	0.89-1.01	32-34	30-32	2.5-3.5	2-3	11-12.5	< 1.5	< 0.1	3-4	6-7

A batch of 19 g of ground mold powder was melted and superheated to 1300ºC in a graphite crucible heated by induction. After maintaining for 5 minutes the molten slag was poured into a brass mold at ~100ºC; this temperature was chosen to ensure that the material solidified fully glassy and without experiencing thermal shock. Each rod was cut into disks of ~3.1 mm thickness by ~13.8 mm diameter. Rods exhibiting any crystallization on the surface were discarded. Figure 2(a) shows the brass mold together with a poured glass rod and examples of a fully glassy and a crystallized disk.

Differential Thermal Analysis Method

A DTA/TGA apparatus (Pyris Diamond, Perkin-Elmer Inc., Waltham, MA) was used to obtain the devitrification peaks of glass samples heated from room temperature to ~1090°C at different heating rates. The molten samples were held for 20 min at that temperature and then cooled at different rates to obtain the crystallization peaks. The upper temperature and holding time were selected to minimize weight loss of the samples. The heating and cooling rates employed in the consecutive devitrification and crystallization tests are given in the plots showing the DTA curves. When the programmed cooling rate did not match the actual rate, a time average around the crystallization peak(s) is reported. For all the tests the glass powder employed was obtained by grinding glass disks to sizes between -230 to +270 meshes (i.e., between -63 to +53 μm). The experiments were conducted in Pt containers in a static air atmosphere and using high purity (99.999%) Al_2O_3 as a reference material supplied by Perkin-Elmer. The apparatus was periodically calibrated using In, Zn, Au and $CuSO_4 \cdot 5H_2O$ standards. The weight of the glass samples loaded to the containers was between 14.95 and 15.05 mg.

Isothermal Treatments

To heat treat the glass disks under isothermal conditions an Inconel 601 circular plate was inductively heated using a 5 kW high frequency (HF) generator (Luzars URF-5, ASEPSA S.A. de C.V., QRO, Mexico) with a three turn flat induction coil. The heating arrangement is shown in Fig. 2(b); the heating plate was placed in the center of the coil and was instrumented with a K-type thermocouple connected to a controller interfaced to the HF generator. The controller was programmed to make the plate follow prescribed thermal trajectories, such as those presented in Figure 3(a). The plate was heated from room temperature to 300°C in 30 s and held for 60 s. This temperature plateau was required to avoid thermal shock of the sample and it did not cause any crystallization of the glass disk. The plate was then heated to the final isothermal treatment temperature in 13 s, independently of the isothermal temperature prescribed. The temperatures and times of the treatment plateaus are given in the Section Validation of the Predicted TTT Curves.

(a)

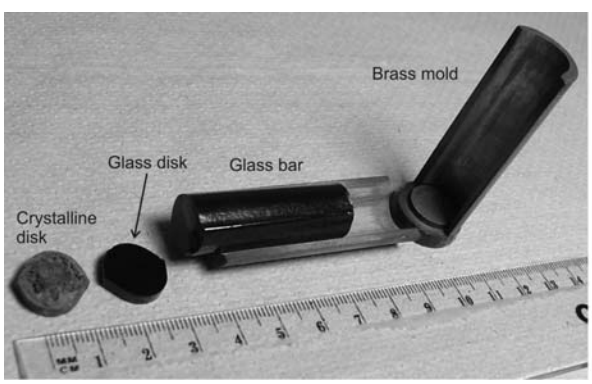

(b)

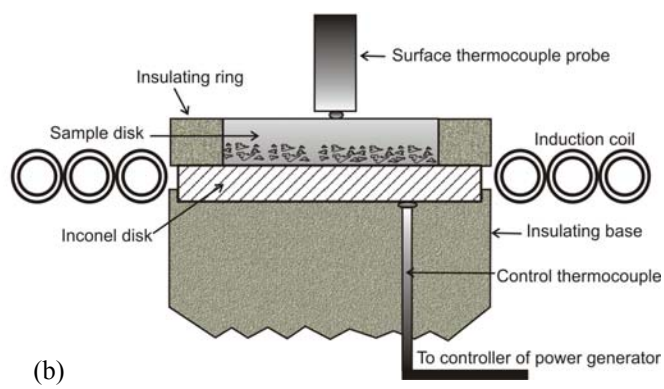

Fig. 2 – (a) Brass mold for casting glass bars and (b) heating arrangement for isothermal treatment tests.

Before starting each heat treatment experiment, the Inconel plate was polished with emery papers 800 and 1200 and the transverse surfaces of the glass disks were polished up to colloidal silica suspension of 0.05 μm. To initiate an experiment a glass disk fitted with a thermally insulating ceramic ring was placed on the hot plate. With the disk in place a contact thermocouple was seated on its upper

surface. Measurement of this surface temperature allowed estimation of the thermal evolution of the disk for calculating the thickness of the region approaching isothermal conditions. This region was predicted to be no more than 10°C below the isothermal treatment temperature when the hot plate reached it. Figure 3(b) shows predicted temperature profiles through the thickness of the disk at two times during the isothermal treatment stage. These calculations are important to accurately define where the metallographic analysis should be done, in order to follow the progress of crystallization under nearly isothermal conditions. The heat conduction model developed for doing the predictions is described elsewhere.[24] After the isothermal treatment, the sample was removed rapidly, 2-3 s, from the heating plate and put to cool on top of a quartz plate at room temperature, without the ceramic ring and while air was blown gently.

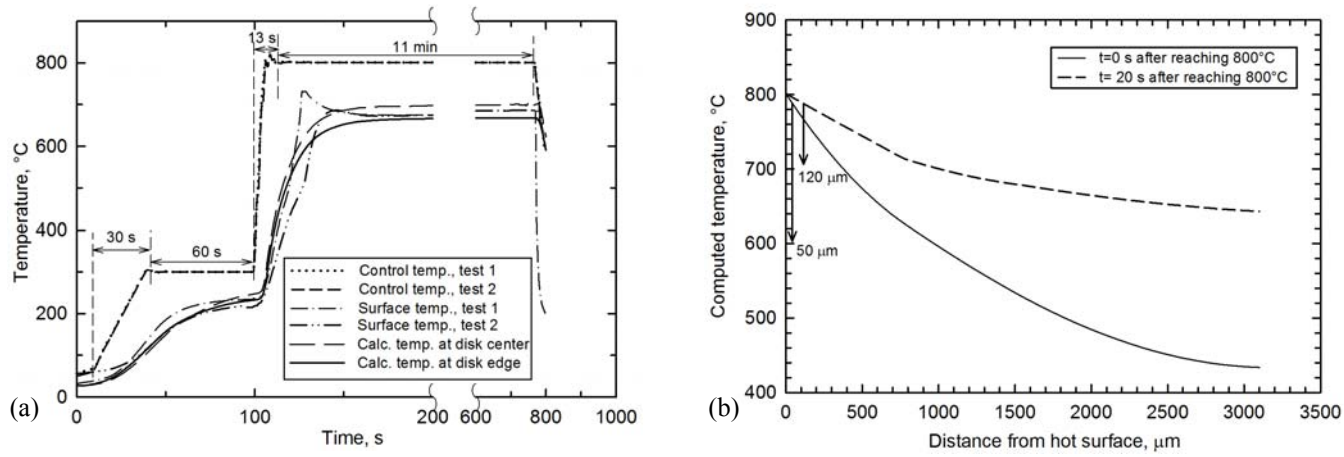

Fig. 3 – (a) Temperature history of hot plate (control temperature), upper surface of disk (surface temperature) and model predictions and (b) variation of temperature with thickness position at the start of the isothermal plateau and 20 s later. An 800ºC treatment plateau lasting 11 minutes is presented.

For metallographic observation the treated disks were mounted in an epoxy resin, afterwards they were cut through the longitudinal middle plane to be able to observe both the longitudinal and the transverse (i.e., surface seated on the hot plate) surfaces. The transverse surface was minimally rough down to avoid removing material that had been in contact with the hot plate. On the other hand the longitudinal surface was polished up to colloidal silica suspension of 0.05 μm and etched for 3 s with a Nital 2 % solution. The samples were observed in stereoscopic and scanning electron microscopes (SEM). The zones analyzed by SEM were within 50 μm to 120 μm of the hot face ensuring that isothermal conditions were met.

RESULTS AND DISCUSSION

DTA Results and Kinetic Parameters for Devitrification and Crystallization Reactions

DTA curves for mold powders A and B are shown in Figs. 4(a) and 4(b), respectively, for various heating rates. Devitrification trajectories from 400°C to ~1090°C and crystallization trajectories in the opposite direction are shown; to distinguish between both paths lines of the same type but different thickness are employed in the figures. As seen in Fig. 4(a) powder A exhibited only one exothermic peak in the temperature ranges covered during devitrification and crystallization and powder B presented two peaks that are very well defined along devitrification, but the second peak appeared only subtly at a cooling rate of -30°C/min during crystallization, as it is observed in Figure 4(b). During devitrification the second peak was already small and in the course of crystallization did not always showed up by the reasons[17] indicated in the Introduction. For powder A the peak corresponded to the formation of cuspidine and for mold powder B the higher peak corresponded also to this mineral and the shorter one to combeite.[24] In the case of powder A a magnification of the traces corresponding only to the temperature range of the crystallization peak is shown as an inset. Since different crystallization conditions such as heating rate, particle size[25] and nucleation temperatures will cause variations in the DTA curves, as mentioned above the glass used for each of the powders was treated similarly and had the same granulometry (between 53 to 63μm). Therefore, the shift exhibited by the DTA curves was associated to the different heating rates used in the experiments. In devitrification the exothermic peak shifted to higher temperatures and became taller with increasing heating rate, while in crystallization the peak shifted to lower temperatures but also became higher with increasing cooling rate. As was indicated in the classical studies of Kissinger[26,27] this variation of the peak with the heating rate, if all other experimental conditions are maintained constant, indicates that the reaction rate varies with temperature, i.e., the reaction requires an activation energy to proceed.

The Kissinger equation[27] which relates the kinetic parameters for a transformation reaction is given as,

$$\ln\frac{\phi}{T_m^2} = \left(\ln(An(1-x_m)^{n-1}) - \ln(\frac{E}{R})\right) - \frac{E}{R}\left(\frac{1}{T_m}\right) \quad (1)$$

where T_m and x_m are the temperature and the fraction of material reacted at the peak, ϕ the heating or cooling rate, n, A, E are the empirical order of reaction, frequency factor and activation energy for crystals formation, respectively, and R the gas constant. The crystalline fraction formed when the maximum of the transformation rate is reached was obtained by graphical integration of the area below the DTA curve up to getting T_m. The T_m values arising to different cooling rates are displayed in Figures 4(a) and 4(b). Since the transformation peaks for both powders are basically symmetric, as observed in the inset (a´) of Fig. 4(a), the fraction x_m was determined to be very close to an average value of 0.5. The order of reaction n was evaluated from the relation obtained by Kissinger, indicating that,

$$n = 1.26\, S^{1/2} \tag{2}$$

where S is the shape index defined as the absolute ratio of the slopes of tangents to the transformation curve at the inflexion points as illustrated in the inset (a'') of Figure 4(a). According to Kissinger equation (1) a plot of $\ln(\phi / T_m^2)$ versus T_m should be a line with a slope $-E/R$ and with an abscissa from which A can be evaluated. The Kissinger lines corresponding to the devitrification of glass samples of powders A and B are displayed in Figure 5 and the legend box includes the values of the kinetic parameters. Thus, it is seen that the formation of crystals during devitrification follows the Kissinger model and that although the energies of activation are quite similar the positions of the lines for the two powders are noticeably different due to the values of A and n, additionally the reproducibility among experiments is quite good. The lines in Fig. 5 appear to demonstrate that under well controlled DTA conditions and sample preparation the positions of the lines, for the devitrification taking place during the heating of mold powder glasses, is controlled by the transformation reaction or reactions resulting from the mold powder nature. The lines obtained for the crystallization occurring during cooling of the mold powder slags are presented elsewhere.[24]

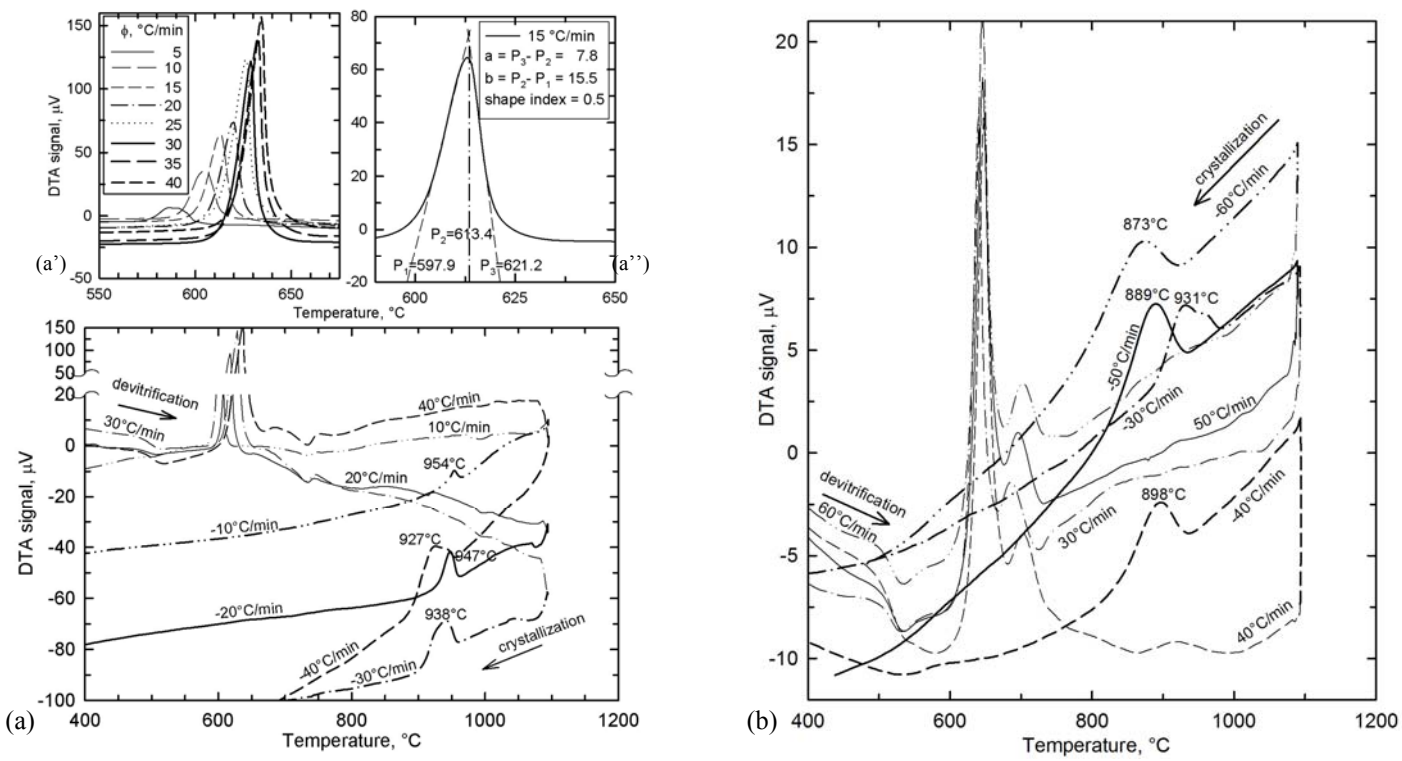

Fig. 4 – DTA heating and cooling curves at different heating and cooling rates for: (a) mold powder A (with insets (a') and (a'')) and (b) mold powder B. Some T_m temperatures are indicated close to the peaks.

New Method for Determining the Rate of Isothermal Transformation for Generating TTT Diagrams

As seen in the previous section the Kissinger method allows obtaining kinetic parameters of phase transformations occurring during non-isothermal conditions. However, to the best of our knowledge this information has not been used to predict the progress of isothermal transformations as a function of time. Assuming that the equation used by Kissinger, to describe the kinetics of decomposition reactions of carbonates and hydroxides, is valid also for the crystallization of amorphous materials, then the rate of transformation of a glassy material can be given as,

$$\frac{dx}{dt} = A(1-x)^n e^{-\frac{E}{RT}} = k(1-x)^n \tag{3}$$

where k is a rate constant that depends on temperature and as seen experimentally in the previous section n, A and E are independent of it. Integrating Equation (3) from $t= 0$ to $t= t$ and $x= 0$ to $x= x$, at constant T, then the time t required to obtain a given transformation fraction x, can be written as,

$$t = \left(\frac{1-(1-x)^{1-n}}{k} \right) \left(\frac{1}{1-n} \right) \tag{4}$$

Thus, considering that the onset and conclusion of crystallization are given by the times when $x= 0.01$ and 0.99, respectively, it is possible to calculate the TTT curves for a transformation characterized by particular kinetic parameters.

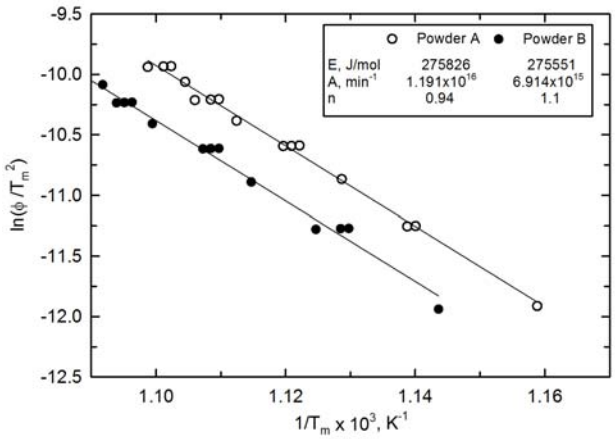

Fig. 5 – Kissinger lines for the devitrification of mold powders A and B. The values of the kinetic parameters are shown in the legend.

Based on the slower cooling rates required for producing the fully glassy rods described in the Sec. Materials and on the results of a heat conduction model[24] regarding the cooling rates prevailing during the solidification of glass disks, it was considered appropriate to introduce in Eq. (4) an incubation time τ, such that,

$$t = \tau + \left(\frac{1-(1-x)^{1-n}}{k} \right) \left(\frac{1}{1-n} \right) \tag{5}$$

For the powders studied a $\tau= 10$ s was specified. The predicted TTT diagrams for powders A and B are represented by the lines plotted in Figures 6 and 7, respectively. The lower parts of the TTT curves were computed from the DTA heating curves, while the upper parts were calculated from the DTA cooling curves, i.e., were computed from devitrification and crystallization DTA tests, respectively. The onset and conclusion of crystallization are indicated by the TTT curves.

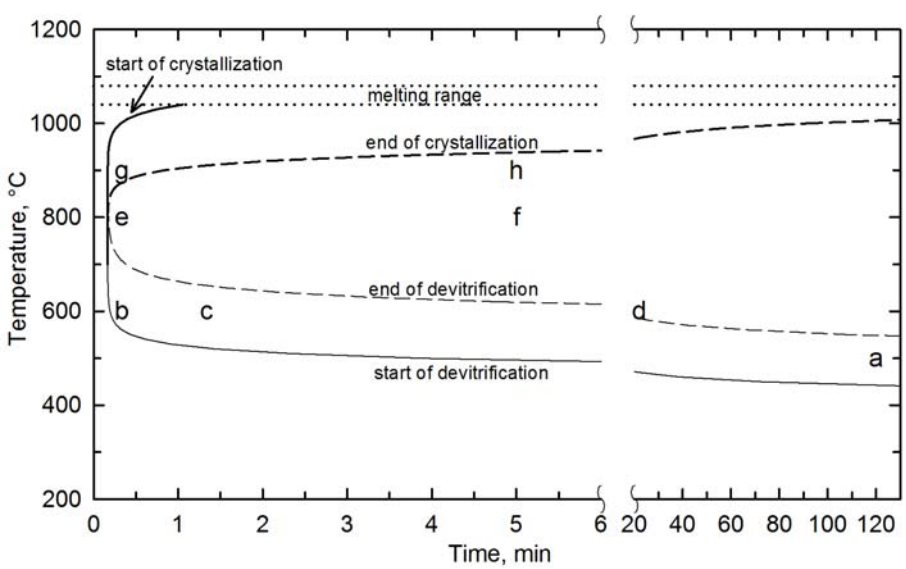

Fig. 6 – TTT diagram for powder A.

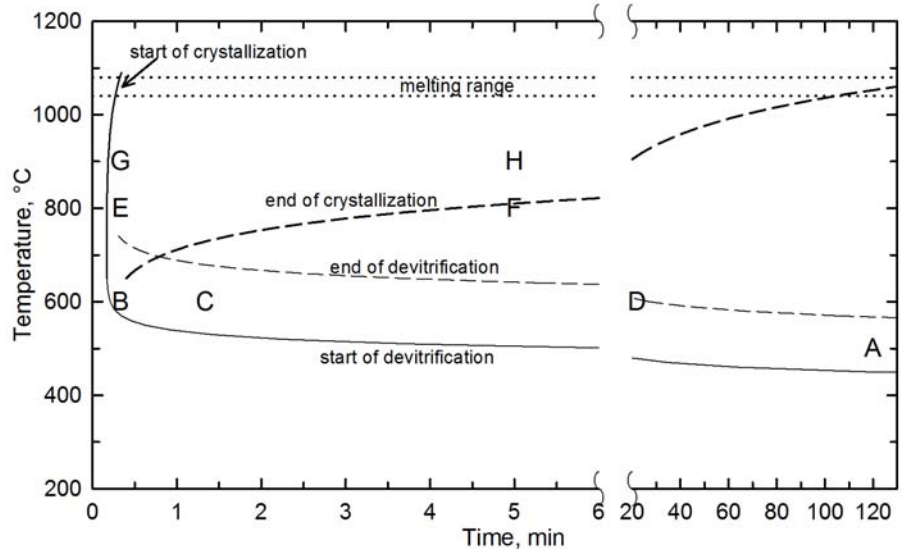

Fig. 7 – TTT diagram for powder B.

The predicted TTT diagrams for both powders are quite similar at temperature below 600°C, but above 700°C they exhibit differences particularly in regard to the conclusion of crystallization; according to the diagrams powder B requires considerably longer times to accomplish crystallization at temperatures between 800ºC and 900ºC. The predicted similarities and differences in the TTT diagrams are validated by the metallographic analysis of isothermally treated disks presented in the following section.

Validation of the Predicted TTT curves

The letters plotted in Figs. 6 and 7 indicate the temperatures and times of the isothermal plateaus at which a thin region of the glass disks was subjected while seated on the hot plate; lowercase letters designate the treatments of mold powder A and uppercase letters those for mold powder B. Corresponding low magnification stereoscopic images of the entire longitudinal cross-section of treated disks together with photomicrographs taken within the isothermal region are displayed in Figures 8 and 9. Agreeing with the TTT diagrams the microstructures *a*, *b*, *c*, and *d* are very similar to those observed in the photomicrographs *A*, *B*, *C* and *D*. As expected from the TTT diagrams the photomicrographs *a*, *b*, *c*, *A*, *B* and *C* show almost completely uniform glassy structures except for some bright spots that appear commonly in samples that are just starting to crystallize. These spots are minute regions, rich in iron, that form early in the process and that possibly act as nucleation sites for cuspidine. Energy dispersive X-ray (EDX) microanalysis spectra of the matrix and of a spot in sample *b* are presented in Figs. 10(a) and 10(b), respectively; spots in samples *a*, *c*, *A*, *B*, and *C* showed similar spectra. As expected from the TTT diagrams the photomicrographs *d* and *D* show very similar and high transformation degrees.

The marked difference in the transformation of powders A and B predicted by the TTT diagrams at 800ºC for conditions *e* and *E* are confirmed by the respective microstructures observed in Figures 8(e) and 9(E). Also, in agreement with the TTT diagrams the microstructures in Figs. 8(f) and 9(F) show a large degree of crystallization in both cases but since this process occurred much faster in mold powder A than B the crystals obtained are much smaller in the first than in the second powder. A behavior similar to this is observed under conditions *g*, *h*, *G* and *H*, but as expected from the TTT diagrams with a smaller degree of crystallization in the case of powder B. For this powder EDX microanalysis spectra of the crystalline and glassy zones are shown in Figures 10(c) and 10(d), the glass zone is rich in Na and poor in Ca.

The TTT diagrams and the isothermal treatments reveal that powders A and B differentiate themselves by their distinct tendency to crystallize at temperatures higher that 800ºC, but below that temperature their behaviors for crystallization are similar. It should be noticed that all the isothermal treatment results were obtained under devitrification conditions and that for temperatures above T_n they were compared with TTT curves generated from DTA cooling curves for crystallization. The agreement of both kinds of results suggests that heating a solid sample to a sufficiently high temperature leads to the same crystallization outcome than cooling of a liquid sample to that temperature. The stereoscopic images included in Figs. 8 and 9 show the different opacity of glass disks treated isothermally at different *T* and *t*. However, low magnifications are not sufficient to judge the tendency of a powder to crystallize.

SUMMARY AND CONCLUSIONS

A novel procedure to calculate Time-Temperature-Transformation (TTT) curves of mold slags is demonstrated in this work. This is based on the integration under isothermal conditions of a Kissinger-type rate equation using rate parameters determined from differential thermal analysis (DTA). The estimated TTT curves agree very well with transformations observed metallographically by inspecting thin glass disks treated isothermally and quenched.

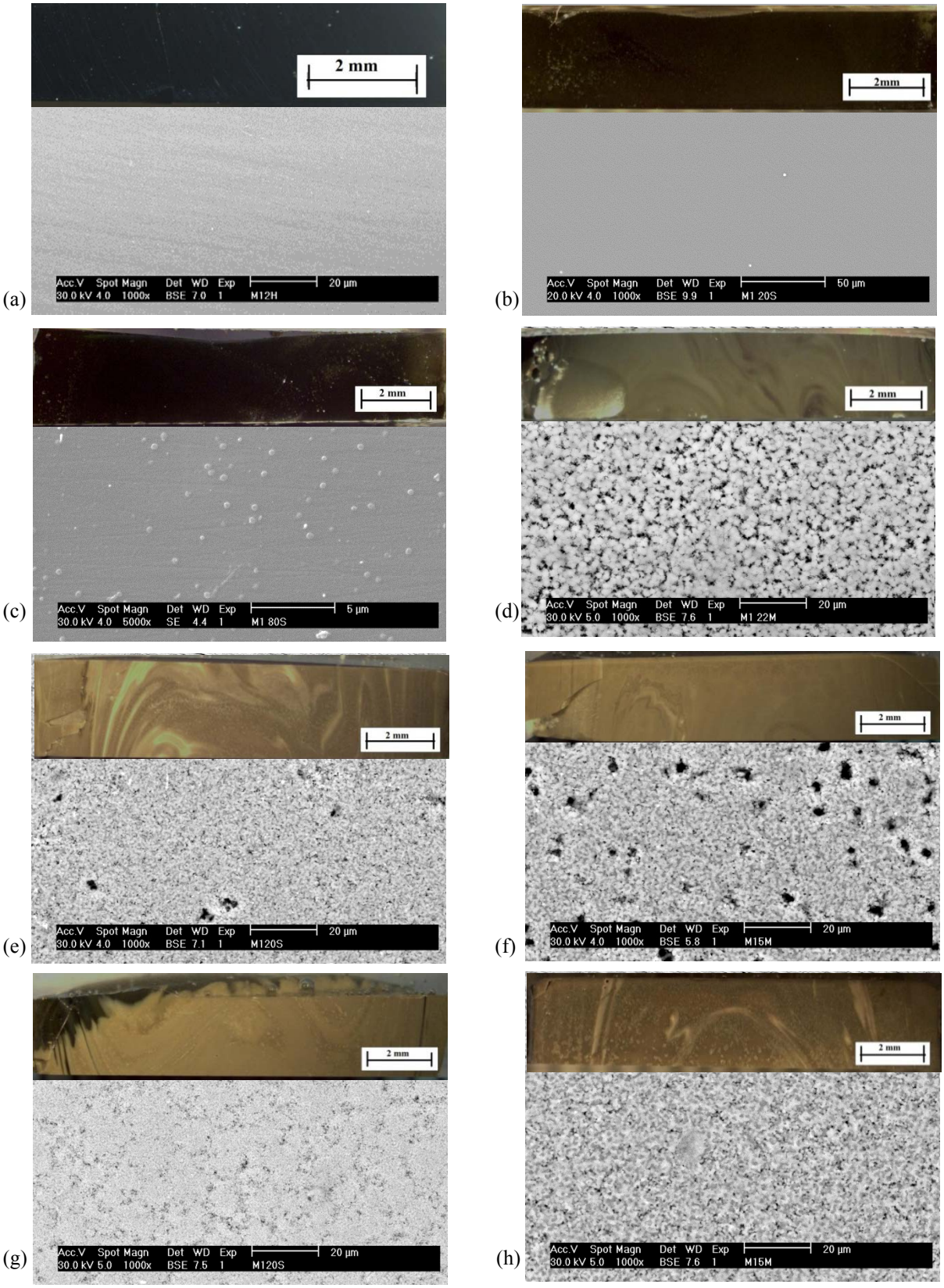

Fig. 8 – Low magnification stereoscopic images and SEM photomicrographs of disks of mold powder A, devitrified under different conditions: (a) 500ºC, 120 min, (b) 600ºC, 20 s, (c) 600ºC, 80 s, (d) 600ºC, 22 min, (e) 800ºC, 20s, (f) 800ºC, 5 min, (g) 900ºC, 20 s and (h) 900ºC, 5 min. The photomicrographs were obtained in back-scattered electrons (BSE) imaging mode, except for (c) where secondary electrons (SE) imaging mode was employed.

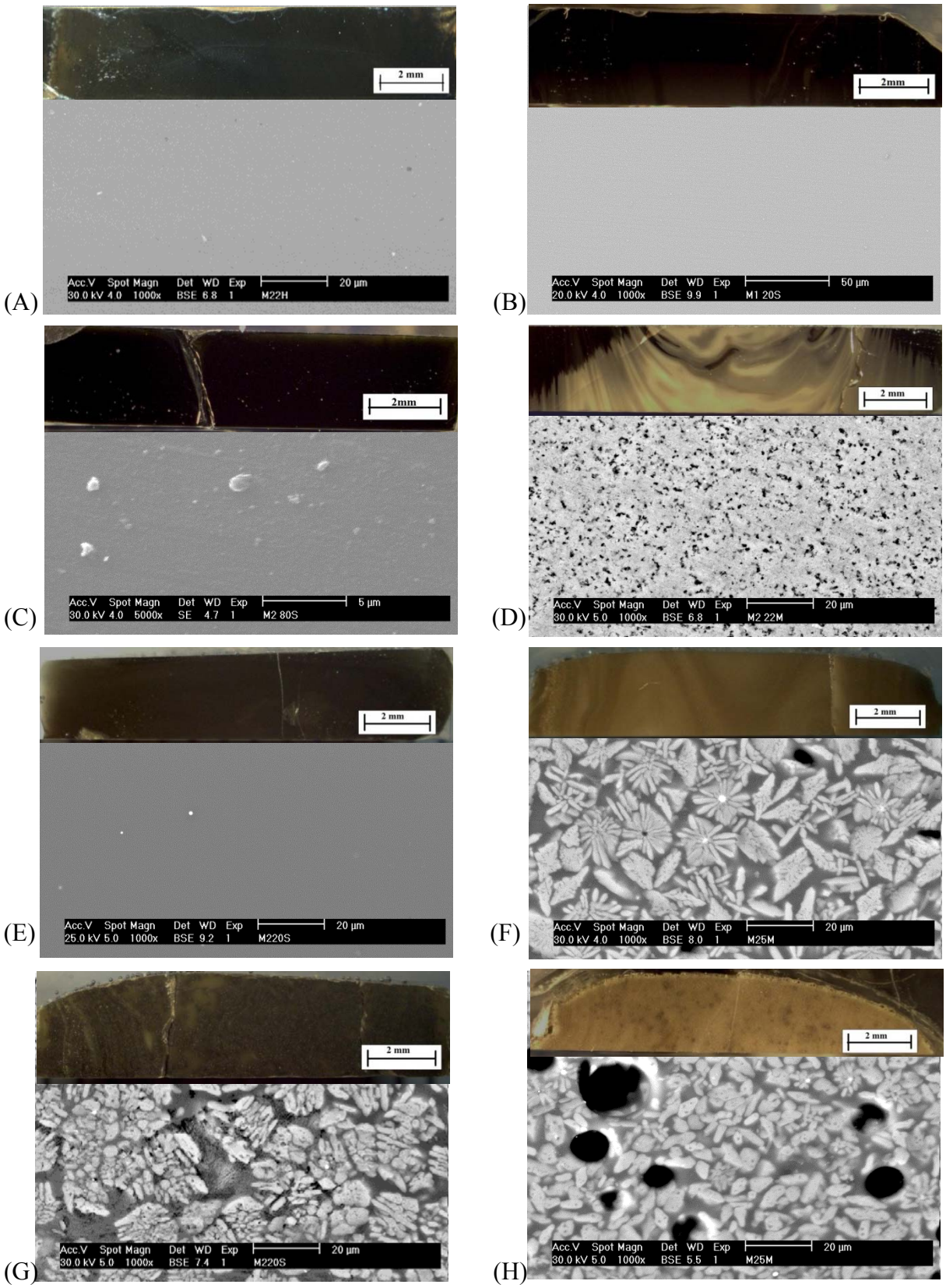

Fig. 9 – Low magnification stereoscopic images and SEM photomicrographs of disks of mold powder B, devitrified under different conditions: (A) 500ºC, 120 min, (B) 600ºC, 20 s, (C) 600ºC, 80 s, (D) 600ºC, 22 min, (E) 800ºC, 20s, (F) 800ºC, 5 min, (G) 900ºC, 20 s and (H) 900ºC, 5 min. The photomicrographs were obtained in back-scattered electrons (BSE) imaging mode, except for (C) where secondary electrons (SE) imaging mode was employed.

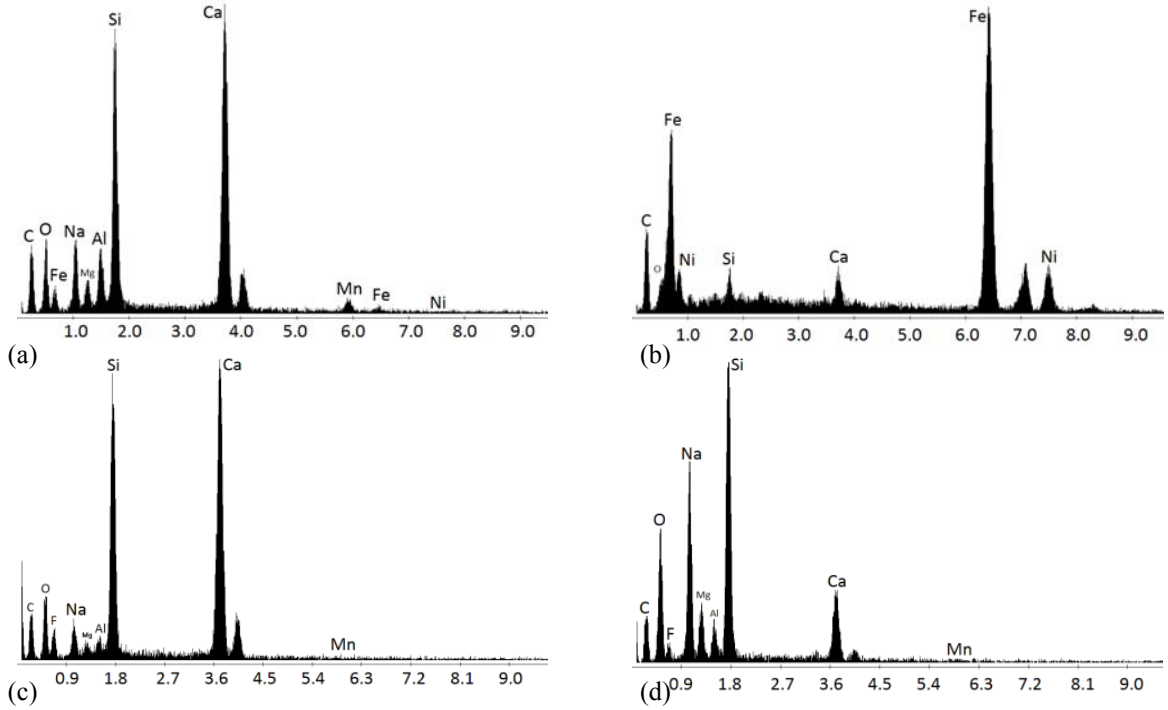

Fig. 10 – Energy dispersive X-ray microanalysis spectra for mold powder A treated at 600ºC for 20 s (Fig. 8(b)): (a) in glass matrix and (b) in small bright spots; for mold powder B treated at 800ºC for 5 min (Fig. 9(F)): (c) in flower shaped crystals and (d) in glass matrix.

ACKNOWLEDGEMENTS

We are grateful to the Centro de Investigación y de Estudios Avanzados (CINVESTAV – Unidad Saltillo) and the Continuous Casting Consortium at the University of Illinois for financial support. YGM is grateful to the National Council of Science and Technology of México (CONACYT) for her Ph.D. scholarship grant.

REFERENCES

1. J.K. Brimacombe and K. Sorimachi, "Crack Formation in the Continuous Casting of Steel", *Met. Trans B.,* 8B, 1977, pp. 489–505.
2. A. Grill, K. Sorimachi and J.K. Brimacombe, "Heat Flow, Gap Formation and Breakouts in the Continuous Casting of Steel Slabs," *Metall. Trans.,* 7B, 1976, pp. 177–189.
3. Y. Meng and B.G. Thomas, ''Simulation of Microstructure and Behavior of Interfacial Mold Slag Layer in Continuous Casting of Steel'', *ISIJ Int.*, 46, 2006, pp. 660-669.
4. R. Bommaraju, ''Optimum Selection and Application of Mold Fluxes for Carbon Steels'', 74*th Steelmaking Conference Proceedings*, Washington, DC, Vol. 74, 1991, pp. 131-146.
5. H. Kyoden, T. Doihara and O. Nomura, ''Development of Mold Powders for High Speed Continuous Casting of Steel'', 69*th Steelmaking Conference Proceedings*, Washington, DC, Vol. 69, 1986, pp.153-159.
6. J.W. Cho and H. Shibata, ''Effect of Solidification of Mold Fluxes on the Heat Transfer in Casting Mold'', *J. of Non Crystalline Solids*, 281, 2001, pp. 110-117.
7. K. Watanabe, M. Suzuky, K. Murakami, H. Kondo and T. Shiomi, ''Development of Mold Powder for High Speed Casting of Middle Carbon Steel'', 79*th Steelmaking Conference Proceedings*, Pittsburgh, PA, Vol. 79, 1996, pp. 265-268.
8. D. Jiang, X. Bing, X. Jianping and JI Chengqing, ''Radiative Heat Transfer in Transition Metal Oxides contained in Mold Fluxes'', *ISIJ Int*., 49, 2009, pp. 1710-1714.
9. S. Feldbauer, I. Jimbo, A. Sharan, K. Shimuzu, W. King, J. Stepanek, J. Harman and A.W. Cramb, ''Physical Properties of Mold Slags that are Relevant to Clean Steel Manufacture'', *78th Steelmaking Conference Proceedings*, Nashvile, Tenn., Vol. 78, 1995, pp. 655-668.
10. J.E. Camporredondo S., A.H. Castillejos E., F.A. Acosta G., E.P. Gutierrez M. and M.A. Herrera G., ''Analysis of Thin Slab Casting by the Compact Strip Process: Part I. Heat Extraction and Solidification'', *Metal. Mat. Trans.*, 35B, 2004, pp. 541-560.
11. I.V. Samarasekera and J.K. Brimacombe, The Thermal Field in Continuous Casting Molds, *Canadian Metall. Q.*, 18, 1979, pp. 251-266.

12. J.J. Montes R., A. Castillejos E., F.A. Acosta G., E.P. Gutiérrez M. and M.A. Herrera G., "Effect of the Operating Conditions of Air-Mists Nozzles on the Thermal Evolution of Continuously Cast Thins Slabs", *Can. Metal. Q.*, Vol. 47, 2008, pp. 187-204.
13. R.J. O'Malley and J. Neal, ''An Examination of Mold Flux Film Structures and Mold gap Behavior Using Mold Thermal Monitoring and Petrographic Analysis at Armco´s Mansfield Operations'', *METEC Congress* 99, Dusseldorf, Vol. 1, 1999, pp. 188-195.
14. P. Rocabois, J.N. Pontoire, J. Lehmann and H. Gaye, ''Crystallization kinetics of Al_2O_3-CaO-SiO_2 Based Oxide Inclusions'', *J. of Non-Crystalline Solids*, 282, 2001, pp. 98-109.
15. Y. Kashiwaya, C.E. Cicutti, A.W. Cramb and K. Ishii, ''Development of Double and Single Hot Thermocouple Technique for in Situ Onsrvation and Measurement of Mold Slag Crystallization'', *ISIJ Int.,* 38, 1998, pp. 348-356.
16. W. Guang-hua, l. Hui and T. Ping, ''CCT and TTT Diagrams to Characterize Crystallization Behavior of Mold Fluxes'', *J. of Iron and Steel Research*, 15, 2008, pp. 32-37.
17. Y. Meng, B.G. Thomas, A.A. Polycarpou, A. Prasad and H. Henein, ''Mould Slag Property Measurements to Characterize CC Mould - Shell Gap Phenomena'', Canadian Metallurgical Quarterly, 45, 2006, pp. 79-94.
18. C.S. Ray, S.T. Reis, R.K. Brow, W. Höland and V. Rheinberger, ''A New DTA Method for Measuring Critical Cooling Rate for Glass Formation'', *J. of Non-Crystalline Solids*, 351, 2005, pp. 1350-1358.
19. M. Dipiaggi, G. Artroli, C. Righi and R. Carli, ''High Temperature Reactions in Molten Flux Slags: Kinetic versus Composition Control'', *J. of Non-Crystalline* Solids, 353, 2007, 2852-2860.
20. K.C. Mills, L. Courtney, A.B. Fox, B. Harris, Z. Idoyaga and M.J. Richardson, ''The use of Thermal Analysis in the Determination of the Crystalline Fraction of Slags Films'', *Termochimica Acta*, 391, 2002, pp. 175-184.
21. F. Neumann, J. Neal, M.A. Pedroza, A.H. Castillejos E. and F.A. Acosta G., Mold Fluxes for High Speed Slab Casting, 79*th Steelmaking Conference Proceedings*, Pittsburgh, PA, Vol. 79, 1996, 249-257.
22. D. Blevins, M. Ingold, A. Schaefer, J. Neal, F. Neumann and C. Sowa, ''Mold Powder Performance: Steel Dynamics' High Speed Thin Slab Casters'', Ironmaking Steelmaking, 27, 2000, pp.85-88.
23. J.A. Kromhout, S. Melzer, E.W. Zinngrebe, A.A. Kamperman and R. Boom, Mould Powder Requirements for High Speed Casting, *Steel Research Int*., 79, 2008, pp. 143-148.
24. Y.G. Maldonado, 3rd Ph.D. Progress Report, CINVESTAV – Unidad Saltillo, Coahuila, México, 2011.
25. W. Li and B.S. Mitchell, ''Nucleation and Crystallization in Calcium Aluminate Glasses'', *J. of Non-Crystalline Solids*, 255, 1999, pp. 199-207.
26. H.E. Kissinger, ''Variation of Peak Temperature with Heating Rate in Differential Thermal Analysis'', *J. of Research of the National Burea of Standards*, 57, 1956, pp. 217-221.
27. H.E. Kissinger, ''Reactions Kinetics in Differential Thermal Analysis'', *Analytical Chemistry*, 29, 1957, pp. 1702-1706.